JOURNAL OF THERMOPHYSICS AND HEAT TRANSFER
Vol. 12, No. 4, October–December 1998

Heat Transfer Analysis and Modeling of a Cryogenic Laser Radiometer

B. C. Johnson,* A. R. Kumar,* and Z. M. Zhang†
University of Florida, Gainesville, Florida 32611
and
D. J. Livigni,‡ C. L. Cromer,§ and T. R. Scott§
National Institute of Standards and Technology, Boulder, Colorado 80303

This study investigates the laser optimized cryogenic radiometer (LOCR) recently acquired by the National Institute of Standards and Technology in Boulder, Colorado, to calibrate laser power meters and detectors. The objectives are to evaluate potentially significant sources of uncertainty in the radiometric measurements and to develop transient models that efficiently and accurately predict the behavior of this radiometer. The analysis suggests that radiation from the Brewster window assembly may cause the total power entering the radiometer to drift more than 130 nW for a room temperature variation of 0.2 K. Steady-state modeling of the LOCR with finite element analysis software indicates a relative inequivalence between optical and electrical heating of 4×10^{-6} at the 1-mW power level. A new thermal model has been developed to simplify transient predictions by combining lumped parameter and one-dimensional elements. This model outperforms single-time-constant exponential models and can be expanded to simulate the complete radiometer system.

Nomenclature

A_c = cross-sectional area of the heat link, cm^2
A_r = receiver surface area, cm^2
C_h = total heat capacity of the heat link, J/K
C_r = total heat capacity of the receiver, J/K
d = receiver length in the analytical model, cm
Fo = Fourier number, $\alpha_s t/L_e^2$
F_{31} = view factor from the outer cryostat aperture to the receiver
k_c = thermal conductivity of copper, W cm^{-1} K^{-1}
k_s = thermal conductivity of stainless steel, W cm^{-1} K^{-1}
$\bar{k}_s$ = average thermal conductivity of the heat link, W cm^{-1} K^{-1}
L = exposed length of the heat link, cm
L_e = equivalent length of the heat link, $L + \Delta x$, cm
N = inequivalence, Eq. (4)
P_E = receiver electrical power input, W
P_L = laser power input, W
q = heat transfer rate, W
q_c = heat transfer by conduction, W
q_r = heat transfer by radiation, W
R = steady-state responsivity, K/mW
T_{He} = liquid helium saturation temperature, K
T_{HS} = heat sink temperature, K
T_h = heat link temperature, K
T_r = receiver temperature, K
t = time, s
x = axial position along the receiver, cm
$\bar{x}$ = normalized axial position along the heat link, $(x + L_e)/L_e$
α_c = thermal diffusivity of copper, cm^2/s
α_s = thermal diffusivity of stainless steel, cm^2/s
Δx = incremental length aded to the heat sink in the transient model, cm
δT = room temperature variation, K
ε = emissivity of the metallic surfaces inside the cryostat
θ_h = relative temperature, $T_h - T_{HS}$, K
θ_r = relative temperature, $T_r - T_{HS}$, K
ξ_n = eigenvalue of the analytical model
σ = Stefan–Boltzmann constant, 5.67×10^{-8} W m^{-2} K^{-4}
τ = time constant, s

I. Introduction

THE laser optimized cryogenic radiometer (LOCR) is a version of the more general class of instruments called absolute cryogenic radiometers (ACRs) that operate just above the saturation temperature of liquid helium and use electrical substitution to measure radiant power traceable to electrical standards. Electrical substitution radiometers (ESRs) using this principle at room temperature have been used to measure the solar constant,[1] solar irradiance,[2] and the Earth's radiation budget.[3] The national measurement laboratories of many countries, including the U.S., now use cryogenic and room-temperature ESRs as primary standards for optical power measurements including the calibration of optical power meters. Mahan et al.[4] applied a finite element model to an ESR to predict its accuracy. Operation of an ESR at cryogenic temperatures began at the National Institute of Standards and Technology (NIST) in the early 1970s to measure thermodynamic temperatures.[5] Pioneering work by Quinn and Martin[6] at the National Physics Laboratory (NPL) in the United Kingdom used the principle to accurately measure the Stefan–Boltzmann constant and compiled a thorough catalog of the potential sources of error in a cryogenic radiometer. Zhang et al.[7] employed finite element analysis (FEA) to model the steady state and transient behavior of the ACR operating at NIST-Gaithersburg in the Low-Background Infrared (LBIR) facility. Their work showed that thermal modeling can help

Presented as Paper 97-3883 at the 32nd National Heat Transfer Conference, Baltimore, MD, Aug. 10–12, 1997; received Dec. 8, 1997; revision received May 8, 1998; accepted for publication May 11, 1998.

*Graduate Research Assistant, Department of Mechanical Engineering.
†Assistant Professor, Department of Mechanical Engineering. Senior Member AIAA.
‡Electrical Engineer, Sources and Detectors Group of the Optoelectronics Division.
§Supervisory Physicist, Sources and Detectors Group of the Optoelectronics Division.

gain a better understanding of the mechanisms underlying cryogenic radiometers, provide performance assessments, and point out directions for future improvement.

Most of the ACRs presently in use serve as primary standards for optical and radiant power measurements in national laboratories around the world, a role that capitalizes on an uncertainty budget typically near 0.02%. Operation of a radiometric standard requires a detailed evaluation of its uncertainty and the prediction of several performance parameters before it can be effectively employed. The unmatched accuracy of an ACR means its performance must be characterized primarily by theoretical modeling instead of comparisons to other instruments. This paper seeks to 1) evaluate error caused by drift in the temperature of the Brewster window assembly, 2) determine the inequivalence between the optical and electrical heating, 3) determine the steady-state responsivity with a finite element model, and 4) develop a simplified finite element model for transient analysis.

An ESR is designed so that equal electrical and radiant power inputs cause nearly identical reactions in the temperature sensor, which allows the radiant power input to be determined from the precisely measured electrical power input. This is accomplished with the general design principles illustrated by the schematic diagram in Fig. 1. In the active mode of operation used during calibrations, both the receiver and the heat sink are maintained at set temperatures by electrical heat inputs. When the shutter is opened, the laser input begins to heat the receiver, and the receiver temperature controller reduces the electrical power to compensate and maintain the set temperature. When the receiver temperature stabilizes at its set value, the electrical power input to the receiver has been reduced by an amount equal to the absorbed laser power. The power of the laser can then be calculated by taking into account the optical absorptance of the cavity and the transmittance of the window that admits the laser beam into the receiver. An ESR may also be operated passively by applying the electrical power input and the laser power input separately. Once the steady-state receiver temperature resulting from laser-induced heating has been determined, the shutter is closed and electrical heating is applied to bring the receiver to the same temperature. In this case, the absorbed laser power is equal to the steady-state electrical power input.

Cryogenic operation improves the accuracy of the electrical substitution technique in several ways. Oxygen-free high-conductivity (OFHC) copper has a very low specific heat at cryogenic temperatures and a correspondingly high thermal diffusivity; forming the receiver from OFHC copper practically eliminates temperature gradients that degrade the equivalence of the electrical and laser heating. The low heat capacity of a copper receiver shortens the time required to reach steady state, which reduces measurement time and decreases the effects of any long-term drift in the boundary conditions. The high-vacuum, low-temperature conditions inside the cryostat make conduction through the heat link the dominant mode of heat transfer, reducing the uncertainty caused by convective and radiative heat transfer. Finally, superconducting wires may be used to eliminate Joule heating in the leads. The LOCR uses niobium–titanium (Nb–Ti) wires, which are superconductive below 9 K.

II. Apparatus

A sectioned view of the LOCR model is shown in Fig. 2. The stainless-steel bolt and washer arrangement forms a resistance that thermally isolates the heat sink from the liquid helium (LHe) well of the cryostat. The low conductivity of the stainless steel and the contact resistance of the construction create a temperature difference between the heat sink and cryostat of approximately 0.18 K for 1 mW of power applied to the heat sink. Because the heat sink consists of OFHC copper for improved temperature uniformity, the thin film resistance heater on the heat sink is used in a servoloop to maintain a stable heat sink temperature despite variations in the cryostat temperature. The servoloop employs a calibrated germanium resistance thermometer (GRT) to measure the temperature and digital electronics to control the temperature.

The heat link consists of a stainless-steel cylinder 4 cm long with an i.d. of 1.45 cm and an o.d. of 1.60 cm. The heat link is clamped between the two halves of the heat sink, with a length $L = 1.27$ cm protruding past the front edge of the heat sink. Isolated by the heat link, the copper receiver is maintained at a nearly uniform temperature by a second temperature control circuit connected to a bare GRT and a thin-film electrical heater mounted on the rear surface of the receiver. The receiver is a cylindrical cavity approximately 6.2 cm long and 1.1 cm in diameter, with a flat rear surface tilted at 33.4 deg to increase the absorptance of the cavity. The inner surface is coated with a specular black paint. The paint has an absorptance of greater than 0.9 and a diffuse reflectance of less than 0.01 in the spectral region from 0.5 to 40 μm.[8] The incoming radiation is admitted through a series of apertures in the radiation shields of the cryostat. A fused-silica window oriented at the Brewster angle is used for maximum transmittance of laser beam with the electric field polarized parallel to the plane of incidence.[9]

The thermal conductivity of the stainless steel is taken from Touloukian et al.,[10] whereas the thermal conductivity of the copper, the density of the stainless steel, and the density of the copper are from Jensen et al.[11] The specific heats of the copper and stainless steel are from Touloukian and Buyco.[12] The specific heat of the black paint is provided by the manufacturer of the LOCR. The thermal conductivity of the paint at cryogenic temperatures is unknown, so it was arbitrarily assigned the same values as the stainless steel. This causes little error because no loads are applied to the paint in the model and it is external to the heat path between any points of interest and the heat sink. Hence, it merely adds thermal mass to the tran-

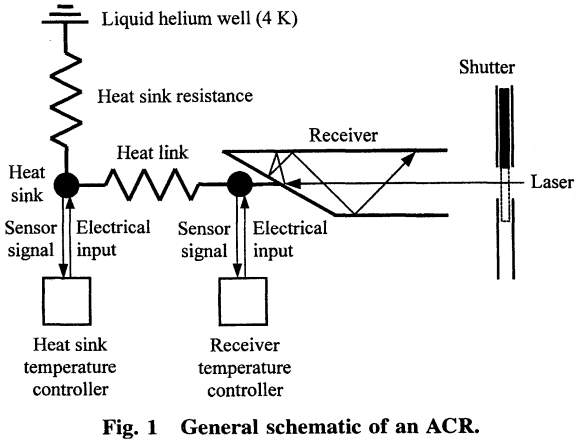

Fig. 1 General schematic of an ACR.

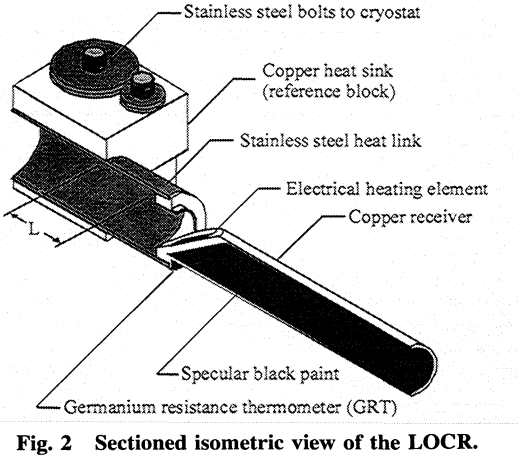

Fig. 2 Sectioned isometric view of the LOCR.

sient calculations and does not affect the temperature distribution.

III. Analysis

A. Modeling Simplifications and Assumptions

The interior of the cryostat is maintained at a high vacuum (5×10^{-6} Pa), which essentially eliminates convection as a means of heat transfer. The ratio of conductive heat transfer (q_c) to the radiative heat transfer (q_r) between the exterior surfaces of the receiver and the interior heat shields of the cryostat is[9]

$$\frac{q_c}{q_r} = \frac{k_s A_c (T_r - T_{HS})/L}{\varepsilon \sigma A_s (T_r^4 - T_{He}^4)} \quad (1)$$

The metal surfaces of the radiometer and cryostat are gold-coated, and at cryogenic temperatures, the emissivity ε is less than 0.02.[13] With the receiver at a temperature of 6 K, the heat sink at 4.76 K, and the LHe well at 4.05 K, the conduction heat transfer is approximately 6×10^5 times as large as the radiative exchange. Consequently, the exterior of the model is assumed to be adiabatic. In reality, the thermal radiation from the window assembly can reach the walls of the receiver, but this is treated separately as an uncertainty (see Sec. IV.A).

The leads to the heater and GRT on the receiver are made of 50-μm-thick Nb–Ti superconducting wires. With no electrical resistance at the operating temperature, they generate no heat and act instead as an alternate conduction path from the receiver to the heat sink. The heat link has a thermal conductance 18,300 times as large as the total conductance of the leads calculated using the thermal conductivity values of Nb–Ti.[14] With little heat passing through the leads, this heat path has a negligible effect on the temperature distribution of the receiver and is omitted entirely. The heat capacities of the leads, heating element, GRT, solder, and epoxy are negligible compared to the copper, paint, and stainless steel; therefore, they are omitted in this study. Similar assumptions were made in the study of Zhang et al.[7]

The most troublesome simplification needed in the model is the assumption of zero contact resistance. The copper receiver and the stainless-steel heat link are held together with a silver solder to improve thermal contact, but the heat link and the heat sink are simply clamped together. The value of the contact resistance depends on the pressure distribution at the interface and surface conditions,[15] which can only be determined experimentally. The imperfect contact between the copper heat sink and the stainless-steel tube may practically extend the length of the heat link. It should be noted that, although the contact resistance complicates the modeling efforts, it does not introduce uncertainty in the measurement. In the present model the contact resistance is neglected because of insufficient information; the assumption may result in a smaller value of the predicted steady-state responsivity. Improved models will be developed after more detailed experimental measurements are done.

B. Finite Element Model

This analysis is performed with a commercial FEA software,[16] on a personal computer. The objective of the FEA model is to simulate the important features of the radiometer while minimizing the required computation time. To better approximate the curved surfaces of the radiometer it is necessary to use second-order three-dimensional elements with a middle node between the corner nodes on each side, as illustrated in Fig. 3. This allows the FEA software to fit a parabolic shape to the locations of the three nodes, creating an element whose actual cross-sectional area matches the calculated area to within 0.0006%.

The receiver and heat link are formed from 20-node hexahedral elements and 10-node tetrahedral elements, whereas the

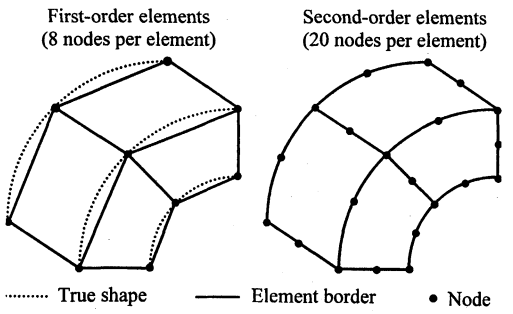

Fig. 3 Comparison of first- and second-order elements.

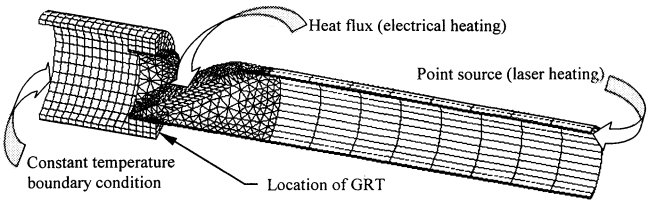

Fig. 4 Complete finite element model.

absorbing paint is represented for four-node shell elements. The final model takes advantage of bilateral symmetry and consists of 4532 elements and 10,441 nodes, as shown in Fig. 4.

Variable thermophysical properties were input to the FEA software as tables of discrete data points. The program then calculated properties at specific temperatures by linear interpolation between the given data points. The thermal conductivity of the paint and the densities of all the materials remained constant over the entire temperature range.

The saturation temperature of the liquid helium in the cryostat is governed by the atmospheric pressure; at high altitude in Boulder, the helium temperature is ≈4.05 K. The heat sink temperature is increased to 4.76 K by a nominal 4-mW power input. The heat sink, including the portion of the stainless steel inside it, is maintained at 4.76 K by the temperature controller. The effect of the heat sink was modeled as a constant temperature boundary condition applied to the end of the exposed portion of the heat link projecting from the heat sink. The electrical heat input was applied as a heat flux evenly distributed across the active area of the heating element. The laser power input condition was not directly modeled; instead, a worst-case scenario was simulated where all of the optical power was located at the node farthest from the GRT, allowing an estimate of the largest possible inequivalence.

IV. Results and Discussion

A. Radiation From the Window Assembly

Designed as a nearly perfect absorber, the receiver is sensitive to thermal radiation from the window assembly that admits the laser radiation. The fused-silica window is opaque to infrared radiation from outside the radiometer, but the window assembly (including the window) is at or near room temperature and emits thermal radiation from its inside surface to the receiver cavity. This issue was addressed by Gentile et al. in their work on the High-Accuracy Cryogenic Radiometer (HACR) used at NIST's Gaithersburg, Maryland, facility.[17] They estimated that a 0.1 K drift in the temperature of the window over the time scale of a measurement caused a power fluctuation of 16.9 nW, approximately 0.002% of the 0.8-mW power used for calibration. However, the HACR uses a set of baffles with very small holes as a radiation trap to restrict the view factor (or configuration factor)[9] between the window assembly and the receiver cavity. The view factor between the window and the cavity in the LOCR is somewhat larger.

The length of the window assembly is 36 times the diameter of the outer aperture, separating it from the interior of the

cryostat. This is large enough that the window assembly can be modeled as a blackbody cavity at room temperature. The view factor from the outer aperture (A_3) to the receiver aperture (A_1) is calculated to be $F_{31} = 0.00127$.[18] At a typical room temperature of 296 K, the assembly radiates 48 μW of power directly into the receiver cavity, which is 3.7 times as much as the 13-μW input predicted for the HACR. If this power input stayed constant for the duration of the calibration, there would be no associated error, but a change in the aperture temperature as the room temperature drifts introduces error by varying the power entering the receiver. Because the amount of radiation leaving the radiometer is negligible, the change in receiver power can be determined by

$$\Delta P_{31} = \sigma A_3 F_{31}[(T_{\text{room}} + \delta T)^4 - T_{\text{room}}^4] \tag{2}$$

If the time interval between the laser heating and electrical heating is 15 min, the worst-case change in aperture temperature is $\delta T = 0.2$ K, which yields a power variation of 130 nW according to Eq. (2).

Support for this prediction comes from preliminary experimental measurements taken with the LOCR. The electrical power input required to maintain a constant receiver temperature in the absence of laser heating was measured as a function of time (after the room air conditioning was shut down). The results show that the aperture temperature, measured by a temperature sensor attached to its outside surface, increased almost linearly while the electrical power necessary to maintain a constant receiver temperature demonstrated a corresponding decrease. This decrease is evidence of the increasing radiant power entering the cavity. A linear regression analysis of the data shows that a 0.2 K change in aperture temperature causes a 190 nW change in the radiant power.[19] The theoretical calculation neglects the radiation emitted from the cryostat surfaces at 77 K and the radiation entering the 4-K radiation shield, which is reflected to the outside of the radiometer; these two sources could account for the 60-nW difference.[18]

The temperature drift caused by room temperature radiation exchange is independent of the laser power; at a typical calibration power of 1 mW the uncertainty is 0.019%, but with a laser power of 100 μW the uncertainty is 0.19%. This uncertainty was not included in the 0.02% uncertainty specified by the manufacturer. The effect of the window assembly radiation on the radiometer measurement can be reduced by three methods: carefully controlling the room temperature, shortening the total measurement time, and reducing the view factor between the room temperature components of the cryostat and the radiometer. Isolating the cryostat in a controlled environment can reduce the drift substantially and is the most feasible short-term solution. A faster measurement cycle reduces the total drift in the room temperature over the measurement period, placing a priority on designing a system with a small time constant. Finally, a series of apertures and baffles that minimize the exchange between the environment and the radiometer are necessary for very accurate measurements.

Following this study, Livigni et al.[19] have developed a dual-baseline correction procedure to account for the linear temperature shift during the measurement. They showed that, by shortening the measurement time and using the dual-baseline method, the uncertainty because of radiation from the window assembly can be reduced to 0.003% for a 1-mW laser.

B. Steady-State Modeling

The steady-state responsivity of the radiometer is defined as $R = (T_r - T_{\text{HS}})/P_E$, where P_E is a step power input to the receiver. This responsivity determines the proper set-point temperature for the receiver temperature controller and depends on the input power because of the temperature dependence of the thermal conductivity of the heat link.

The responsivity can be approximated by neglecting any temperature variations over the copper receiver and modeling the exposed portion of the heat link as a one-dimensional steady state conduction problem. If the thermal conductivity of the stainless steel is approximated as a linear function of temperature, then

$$R = L/\bar{k}_s A_c \tag{3}$$

where $\bar{k}_s$ is the thermal conductivity of stainless steel at a mean temperature of 5.25 K. The responsivity is calculated to be 0.93 K/mW using this formula.

A more accurate prediction can be made with a steady-state finite element model, as negligible contact resistance is the only significant assumption made. Electrical power input is used for these calculations because of the ease with which it is applied, but the next paragraph demonstrates that there is no significant difference in the sensor temperature when radiant power is applied. As shown in Fig. 5, the calculated responsivity decreases as the power increases, a trend caused by the increase in thermal conductivity as the temperature rises. The measured data show the same trend, but are about 25% higher.[19] This difference can be attributed to the contact resistance between the heat link and heat sink, which is neglected by the model.

The inequivalence N of the radiometer is the percent difference between the sensor temperatures for equal inputs of electrical and radiant power:

$$N = \frac{T_{\text{laser}} - T_{\text{elec}}}{T_{\text{elec}}} \times 100\% \tag{4}$$

This inequivalence arises because the loads are applied at different locations, resulting in different boundary conditions for the conduction problem. A worst-case estimate of the inequivalence is provided by applying a point source of heat at the extreme end of the receiver and comparing the results to the previously calculated solution with electrical power input. This creates the maximum possible disparity between the two load cases. Because of the adiabatic boundary conditions, at steady state, the receiver is isothermal at points farther from the heat sink than the heat input. Therefore, a sensor located between the electrical heater and the far end of the receiver experiences a greater temperature rise when heat is applied at the end of the receiver than when it is applied at the heater. The inequivalence for various GRT positions along the receiver is shown in Fig. 6, where x is the distance from the base of the receiver. The result indicates that the radiometer performs best when the sensor is located at the base of the receiver. The actual location of the GRT is on the copper ring near the stainless-steel heat link. An average of the temperatures at the position and size of the GRT results in $N = 4 \times 10^{-6}$ at 1 mW. This shows that inequivalence caused by the different spatial distributions between the laser and electrical power is negligible. The effects of cavity absorptance and window transmittance are not included in the analysis, however.

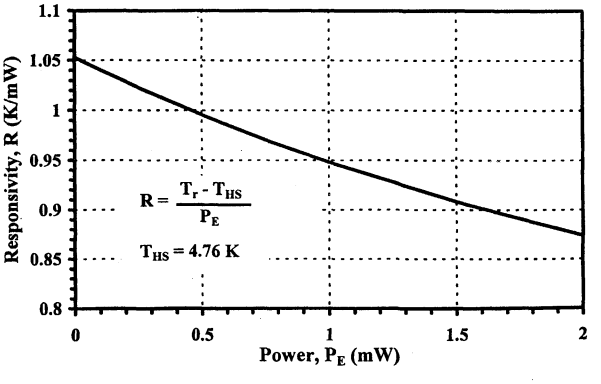

Fig. 5 Calculated steady-state responsivity.

The accuracy of these results can be assessed only indirectly. The FEA software treats the nonlinearity caused by the variable thermophysical properties by iterating with properties evaluated at the previous temperature until successive iterations are within 1×10^{-10} K, using a frontal solver with an accuracy of 1×10^{-9} K each time. Smaller tolerance limits do not change the results. Further mesh refinement does not alter the results because of the use of higher order elements. To verify that this approach gives valid results, the mean temperature of the nodes where the stainless-steel heat link meets the copper receiver can be compared to the value predicted by a one-dimensional conduction analysis of the exposed heat link. Using this method, the finite element model agrees with the analytical results within 0.00213%. Most of this error can be attributed to the one-dimensional approximation, which requires averaging to determine the mean temperature at the junction of the heat link and receiver.

C. Transient Modeling

The most accurate transient analysis applies a different loading and solution procedure to the complete geometry and mesh of the finite element model used in the steady-state analysis. The graph of the sensor temperature vs time in Fig. 7 shows the transient behavior of the radiometer when a step electrical input of 1 μW is applied to the model for 80 s.

A solution to the complete finite element model takes 15–40 h and generates information about thousands of nodes that cannot be compared with the actual radiometer. The only information necessary is the transient history of the sensor. Therefore, it is common practice to model the receiver with a lumped-capacitance model that assumes an isothermal receiver and a heat link with no heat capacity, resulting in a single-term exponential transient temperature profile. The closest fit to the complete model that can be achieved with such a model occurs when a time constant $t = 6.913$ s is chosen, but Fig. 7 shows that the fit is poor for the first few seconds of operation.

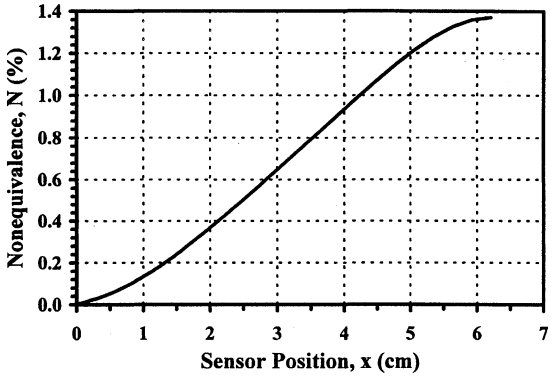

Fig. 6 Inequivalence at 1 mW as a function of sensor position.

A better fit is obtained with a finite element model of reduced complexity. This model, shown in Fig. 8, represents the heat link as a series of one-dimensional stainless-steel conduction elements and the receiver as a collection of thermal mass elements at the last node. Each element of the receiver represents a different material (copper, paint, etc.) with the proper volume and a uniform temperature. The actual radiometer includes a section of the copper receiver inserted inside the stainless-steel heat link (see Fig. 2), breaking the one-dimensional symmetry assumed by the reduced model and adding to the total resistance between the sensor and the heat sink. The majority of this portion of the heat link is at the same temperature as the receiver, but its thermal resistance and thermal mass must be properly accounted for. Therefore, a conduction element of length Δx was added to the heat link, with the remainder of the stainless steel added to the receiver as a mass element. The best match between complete and reduced models was found for $\Delta x = 0.026348$ cm, creating a heat link with an effective length $L_e = 1.2964$ cm. This reduced model has only 33 nodes and can be solved in less than 10 min. The receiver temperature calculated from this model agrees with the complete FEA model within 2 μK, as shown in Fig. 7.

Confirmation of the accuracy of the reduced model comes from a one-dimensional transient analytic model that is valid only for constant thermophysical properties. Because the receiver is later simplified as isothermal, only its total heat capacity is important and it can be approximated as a copper rod with the same cross-sectional area as the heat link, as shown in Fig. 9. The governing equations, initial conditions, and boundary conditions of the analytical model are given in Table 1, where $\theta_h = T_h - T_{HS}$, $\theta_r = T_r - T_{HS}$, and a step heat input q is applied at $x = d$. The first shared boundary condition represents the fact that the temperature distribution is continuous; contact resistance that might cause a discontinuity in the temperature is neglected for reasons discussed in Sec. III.A. The second shared boundary condition represents conservation of energy; the junction between the metals neither stores nor generates heat, so the incoming and outgoing heat fluxes must be equal.

Solution by separation of variables gives lengthy Fourier series for θ_h and θ_r.[18,20] The copper receiver has a much larger thermal diffusivity ($\alpha_c/\alpha_s \approx 10^5$) than the stainless-steel heat link. By approximating the receiver as isothermal and letting

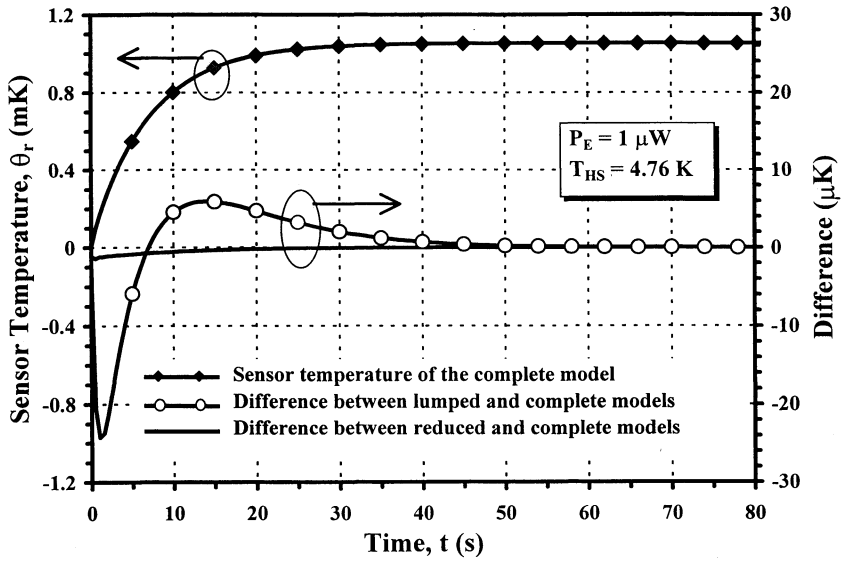

Fig. 7 Comparison of models to the complete finite element model.

Table 1 Analytical model equations

	Heat link	Receiver
Governing equations	$\frac{\partial^2\theta_h}{\partial x^2} = \frac{1}{\alpha_s}\frac{\partial\theta_h}{\partial t}$	$\frac{\partial^2\theta_r}{\partial x^2} = \frac{1}{\alpha_c}\frac{\partial\theta_r}{\partial t}$
Initial conditions	$\theta_h(x, 0) = 0$	$\theta_r(x, 0) = 0$
Boundary conditions	$\theta_h(-L_e, t) = 0$	$-k_c\frac{\partial\theta_r}{\partial x}\Big\|_d = -\frac{q}{A_c}$
	$\theta_h(0, t) = \theta_r(0, t)$	
	$-k_s\frac{\partial\theta_h}{\partial x}\Big\|_0 = -k_c\frac{\partial\theta_r}{\partial x}\Big\|_0$	

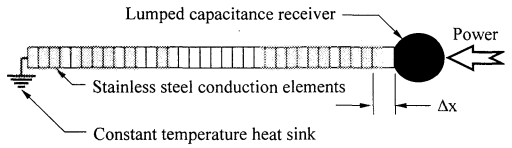

Fig. 8 Schematic of the reduced finite element model.

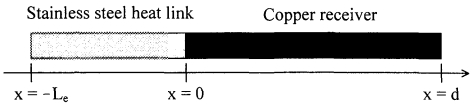

Fig. 9 Analytical model.

$\alpha_c \to \infty$, the temperature distribution in the heat link is derived as follows:

$$\theta_h(\bar{x}, Fo) = \frac{qL_e}{k_s A_c}\left[\bar{x} - 4\sum_{n=1}^{\infty}\frac{\sin\xi_n \exp(-\xi_n^2 Fo)\sin(\xi_n\bar{x})}{\xi_n(2\xi_n + \sin 2\xi_n)}\right] \quad (5)$$

where $\bar{x} = (x + L_e)/L_e$ is the normalized axial position and $Fo = \alpha_s t/L_e^2$ is the Fourier number. The eigenvalues ξ_n are the roots of the equation

$$\xi_n \tan\xi_n = C_h/C_r \quad (6)$$

where C_h and C_r are the heat capacities of the heat link and receiver. Note that $\theta_r(Fo) = \theta_h(1, Fo)$.

Equation (6) was solved by Newton–Raphson iteration for the first six eigenvalues, giving time constants of 7.215, 0.645, 0.199, 0.093, 0.054, and 0.035 s. The exponential term does not decay fast enough to justify a single-term exponential function because the large heat capacity of the heat link (C_h/C_r = 2.136) violates the assumptions of the lumped-capacitance exponential model.

The analytical model and the reduced finite element model, run with constant properties, are compared in Fig. 10 for an 80 s heat input of 1 μW. A small heat input was chosen so that the results would not be affected by the constant property assumption. The graph shows excellent agreement between the two models at all but the shortest times, where the magnitude of the temperature is so small that any difference leads to a large relative error.

While the analytical model discussed earlier is elegant, the restriction to constant thermophysical properties limits its use. The reduced finite element model avoids that limitation and provides a basic framework for future analysis of ACRs. This model can also be used to determine the thermophysical properties of materials at cryogenic temperatures, as demonstrated by Zhang et al.[21] A representation of the heat sink as another lumped mass can be added and linked to a node representing the LHe well of the cryostat with stainless-steel conduction bar elements representing the bolt and washer arrangement of

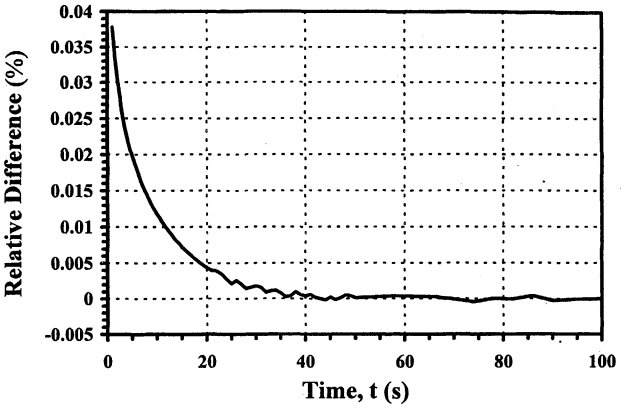

Fig. 10 Relative difference between analytical and reduced models.

the real item. This will allow the time constant of the heat sink and other transient behavior to be estimated and compared to experimental data. The input of the temperature controllers governing the heat sink and receiver can be added in the future as a feedback mechanism to complete the model.

V. Conclusions

This paper presents an analysis of a new cryogenic radiometer, and it accomplishes three major tasks: the evaluation of the thermal radiation from the Brewster window assembly as a potential significant error source, the prediction of parameters important to the operation of the radiometer, and the development of transient models that efficiently and accurately predict the behavior of the instrument. A change of 130 nW in the thermal radiation from the Brewster window assembly to the receiver is predicted over the course of a 0.2-K room temperature drift. For a typical calibration run at 1 mW, this uncertainty is estimated to be 0.013%; low-power measurements are even less accurate. Support for the validity of this calculation is provided by experimental data showing a 190-nW power variation for an aperture temperature drift of 0.2 K. The uncertainty can be significantly reduced with the present instrument by carefully controlling the temperature of the window assembly, shortening the time interval between the laser and electrical heating, and using a dual-baseline correction procedure.

The steady-state responsivity decreases as the applied power increases, a trend explained by the increase in thermal conductivity as the temperature rises. At 1 mW of input, the predicted steady-state responsivity is 0.948 K/mW, which is lower than the experimental value because of contact resistance. Inequivalence is assessed as a function of the sensor position, showing that moving the sensor toward the heat link improves performance. At the actual position of the GRT, the relative inequivalence caused by different spatial distributions between laser and electrical power input is 4×10^{-6} for a 1-mW power input, which is negligibly small.

Transient modeling has been performed for open-mode operation using the complete finite element model to obtain detailed temperature distributions during the heating and cooling periods. It takes more than 10 h to model 120 s of the radiometer operation. The conventional lumped capacitance model ignores the heat capacity of the heat link, which is actually twice as large as that of the receiver, and fails to predict the initial transient behavior. A reduced finite element model has been developed and described in this paper based on the assumption that the temperature gradient on the receiver is negligible. This model agrees well with the complete model in predicting the sensor temperature while shortening the solution time from hours to minutes. An analytical model based on constant thermophysical properties is also developed. Solution of the analytical model by separation of variables yields an

infinite Fourier series of exponential terms, with each term containing a time constant smaller than in the previous term. The results of the analytical model are in excellent agreement with those of the reduced finite element model. The analytical model, however, is limited because the strong temperature dependence of the thermophysical properties of materials at cryogenic temperatures. Another advantage of the reduced finite element model is that it can be expanded in the future to include the heat sink and thermal coupling between the heat sink and the LHe well. Such a model could ultimately improve the temperature control algorithm in cryogenic radiometers.

Acknowledgments

The work at the University of Florida was partially supported by the Optoelectronics Division of the National Institute of Standards and Technology. Valuable discussions with Dave Compertore and Peter Foukal of Cambridge Research and Instrumentation Inc. are greatly appreciated. B.C.J. acknowledges William Tiederman and Jill Peterson for serving on his M.S. thesis committee and for their helpful comments on this work.

References

[1]Frohlich, C., "History of Solar Radiometry and the World Radiometric Reference," *Metrologia*, Vol. 28, No. 3, 1991, pp. 111–115.

[2]Zhang, Z. M., Ge, X. S., and Wang, Y. F., "A Novel Pyrheliometer of High Accuracy," *Solar Energy*, Vol. 29, No. 5, 1987, pp. 371–377.

[3]Mahan, J. R., Tira, N. E., Lee, R. B., and Keynton, R. J., "Comparison of the Measured and Predicted Response of the Earth Radiation Budget Experiment Active Cavity Radiometer During Solar Observations," *Applied Optics*, Vol. 28, No. 7, 1989, pp. 1327–1337.

[4]Mahan, J. R., Kowsary, F., Tira, N. E., and Gardiner, B. D., "Transient Conduction-Radiation Analysis of an Absolute Active Cavity Radiometer Using Finite Elements," *International Symposium on Thermal Problems in Space-Based Systems*, edited by F. Dobran and M. Imber, HTD Vol. 83, American Society of Mechanical Engineers, New York, 1987, pp. 39–47.

[5]Ginnings, D. C., and Reilly, M. L., "Calorimetric Measurement of Thermodynamic Temperatures above 0°C Using Total Blackbody Radiation," *Temperature: Its Measurement and Control in Science and Industry*, edited by H. H. Plumb, Vol. 4, Pt. I, Instrument Society of America, Research Triangle Park, NC, 1972, pp. 339–348.

[6]Quinn, T. J., and Martin, J. E., "A Radiometric Determination of the Stefan-Boltzmann Constant and Thermodynamic Temperatures Between −40°C and +100°C," *Philosophical Transactions of the Royal Society of London A*, Vol. 316, No. 11, 1985, pp. 85–189.

[7]Zhang, Z. M., Datla, R. U., Lorentz, S. R., and Tang, H. C., "Thermal Modeling of Absolute Cryogenic Radiometers," *Journal of Heat Transfer*, Vol. 116, No. 4, 1994, pp. 993–998.

[8]Datla, R. U., Stock, K., Parr, A. C., Hoyt, C. C., Miller, P. J., and Foukal, P. V., "Characterization of an Absolute Cryogenic Radiometer as a Standard Detector for Radiant-Power Measurements," *Applied Optics*, Vol. 31, No. 34, 1992, pp. 7219–7225.

[9]Siegel, R., and Howell, J. R., *Thermal Radiation Heat Transfer*, 3rd ed., Hemisphere, Washington, DC, 1992, Chaps. 4 and 6.

[10]Touloukian, Y. S., Powell, R. W., Ho, C. Y., and Klemens, P. G., "Thermal Conductivity: Metallic Elements and Alloys," *Thermophysical Properties of Matter*, edited by Y. S. Touloukian and C. Y. Ho, Vol. 1, IFI/Plenum, New York, 1970.

[11]Jensen, J. E., Tuttle, W. A., Stewart, R. B., Brechna, H., and Prodell, A. G. (eds.), *Brookhaven National Laboratory Selected Cryogenic Data Notebook*, Vols. 1 and 2, BNL, Upton, NY, 1980, Secs. 7, 8, and 14.

[12]Touloukian, Y. S., and Buyco, E. H., "Specific Heat: Metallic Elements and Alloys," *Thermophysical Properties of Matter*, edited by Y. S. Touloukian and C. Y. Ho, Vol. 4, IFI/Plenum, New York, 1970.

[13]Toscano, W. M., and Crovalho, E. G., "Thermal Radiative Properties of the Noble Metals at Cryogenic Temperatures," *Journal of Heat Transfer*, Vol. 98, No. 3, 1976, pp. 438–445.

[14]Flachbart, K., Feher, A., Janos, S., Malek, Z., and Ryska, A., "Thermal Conductivity of Nb-Ti Alloy in the Low-Temperature Range," *Physica Status Solidi B*, Vol. 85, No. 2, 1978, pp. 545–551.

[15]Mikic, B. B., "Thermal Contact Conductance: Theoretical Considerations," *International Journal of Heat and Mass Transfer*, Vol. 17, No. 3, 1974, pp. 205–214.

[16]ANSYS Version 5.3, ANSYS Inc., Houston, PA, 1996.

[17]Gentile, T. R., Houston, J. M., Hardis, J. E., Cromer, C. L., and Parr, A. C., "National Institute of Standards and Technology High-Accuracy Radiometer," *Applied Optics*, Vol. 35, No. 7, 1996, pp. 1056–1068.

[18]Johnson, B. C., *Heat Transfer Analysis and Modeling of a Cryogenic Laser Radiometer*, M.S. Thesis, Dept. of Mechanical Engineering, Univ. of Florida, Gainesville, FL, Dec. 1997.

[19]Livigni, D. J., Cromer, C. L., Scott, T. R., Johnson, B. C., and Zhang, Z. M., "Characterization of a Cryogenic Radiometer and Intercomparison with a Laser Calorimeter," Absolute Radiometry and Remote Sensing Conf., Oct., Tucson, AZ, 1997.

[20]Ozisik, M. N., *Heat Conduction*, 2nd ed., Wiley, New York, 1993, Chap. 8.

[21]Zhang, Z. M., Lorentz, S. R., Rice, J. P., and Datla, R. U., "Measurement of the Thermophysical Properties of Polyimide and a Black Paint for Future Development of Cryogenic Radiometers," *Metrologia* (to be published).